Experiments computing highly-resolved sea level spectra from dual-satellite altimetry

Edward D. Zaron

College of Earth, Ocean and Atmospheric Science
Oregon State University
edward.d.zaron@oregonstate.edu

Ocean Surface Topography Science Team Meeting
Venice & virtual forum
October 31-November 4, 2022

Motivation & Background

(1) With conventional mono-satellite altimetry data, the highest resolvable frequency of sea level variability is determined by the orbit ground track repeat period. For example, for the TOPEX and Jason missions flying in the reference orbit, the repeat period is approximately 10 days, so the highest resolvable, or Nyquist, frequency is approximately (1/20) cycles-per-day (cpd).

(2) This presentation describes an analysis of dual-satellite altimetry, using data from multiple Jason missions and the CryoSat-2 mission, which seeks to overcome some limitations of mono-satellite altimetry to study variability at frequencies above (1/20) cpd.

(3) By considering sea level differences obtained at the orbit crossovers at multiple times, e.g., Jason-2 at time t_1 minus CryoSat-2 at time t_2, it is possible to investigate sea level variability at higher frequencies, where the Nyquist frequency is determined by the samping interval $\tau = t_1 - t_2$.

The material in this presentation is based on the article, "Baroclinic Tidal Cusps from Satellite Altimetry". (Note: The blue text, at left, is a clickable hyperlink.)

Motivation & Background

(4) My primary interest is to study tidal signals with frequencies near 2 cpd, and my goal is to compute a highly-resolved sea level spectrum which reveals properties of the “tidal cusps”, i.e., sea-level caused by the interactions of the tidal internal waves with mesoscale eddies or other sub-inertial processes. The terms, “tidal cusps”, “non-stationary tides”, “incoherent tides”, and “non-phase-locked tides” are different ways to refer to the phenomenon whereby signals at the tidal carrier frequencies are modulated by other oceanic processes.

(5) The mathematical tool I use to compute spectra is the relationship between the power spectrum and the time-lagged autocovariance function, $C(\tau)$.

The plot at right shows the variogram, $\Gamma(\tau)$, rather than the autocovariance, $C(\tau)$, for the Jason minus CryoSat-2 sea level anomalies. Using all standard corrections (top curve), the variogram is dominated by the low-frequency mesoscale and seasonal variabilities. Subtracting the mesoscale signal (bottom curve), as estimated by the DUACS multi-satellite L4 product, removes most low-frequencies and greatly increases the signal-to-noise for frequency-domain analysis of high-frequency variability.

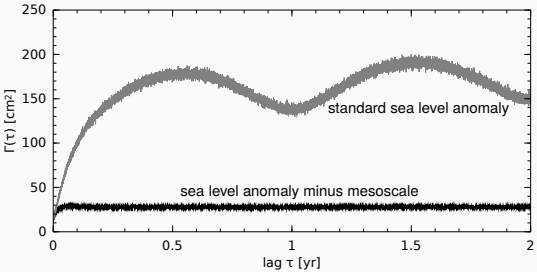

Analysis Methods

(1) Because the variogram, shown above, is estimated by globally averaging data from Jason/CryoSat-2 crossovers at different times, and because the altimeter errors are correlated (due to common path-delay corrections), there are a number of artifacts in the sea level power spectrum which are analyzed in detail in the manuscript linked above.

(2) The power spectrum is estimated from the Fourier transform of the time-lagged autocovariance using lags τ from $1/2$-hour to 2-years, with resolution $\Delta\tau = 1$-hour.

(3) Spectra ("tidal cusps") around the narrow tidal peaks are analyzed by fitting a Lorentzian model to the spectrum to estimate the variance and decorrelation time of the non-phase-locked tidal variability.

The power spectrum of sea level anomaly is estimated (at right). Variance at the astronomically-forced tidal frequencies is unambiguous. Variability at some nonlinear overtides is apparent but of dubious statistical significance.

This spectrum represents the sea level anomaly spectrum with all standard corrections, including the removal of barotropic tides and the mesoscale. The tidal variability which remains is related to baroclinic tides or residual barotropic tides which are not removed by the standard corrections.

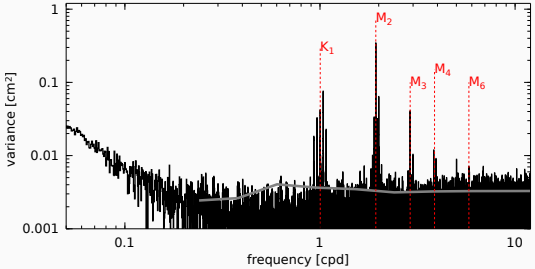

Results: the high-resolution sea level anomaly spectrum

Diurnal Band

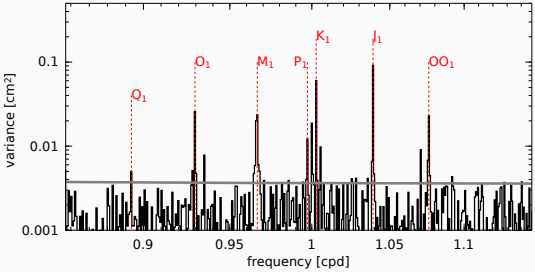

The sea level anomaly spectrum in the diurnal band shows a variety of spectral peaks. Variability at the M_1, OO_1, and J_1 frequencies is likely the result of error in barotropic tidal corrections. Variability at the O_1 and K_1 frequencies likely reflects baroclinic tides generated in the Western Pacific.

Semidiurnal Band

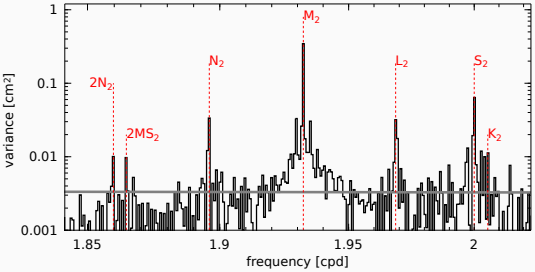

The sea level anomaly spectrum in the semidiurnal band is dominated by the M_2 peak and the continuum of variance which surrounds it. The horizontal gray line in this and the previous figures is the estimated error in the power spectrum. Because the spectrum results from a mixture of deterministic tidal components and random processes, it is shown unsmoothed (it is a variogram) using units of cm^2 variance per Fourier frequency bin.

Results: the M_2 "tidal cusp", i.e., the spectrum of the non-phase-locked tide

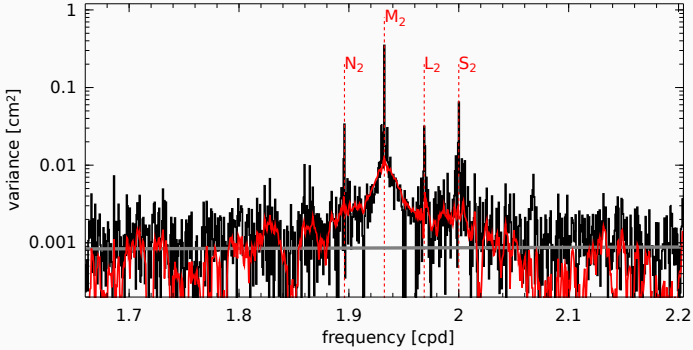

This figure again shows the sea level anomaly spectrum in the semidiurnal band, but note the larger range of frequencies shown as compared to the previous figure. The purpose of showing this larger view is to illustrate the overall width of the tidal cusp in comparison with the frequencies comprising the semidiurnal tidal group.

The red line shows the spectrum of the residual after removing the phase-locked tidal variability. The tidal cusp is now prominent, centered on M_2,

Note that there appears to be an "Inner Lorentzian" characterized by the nearly triangular-shaped residual spectrum close to M_2 (from 1.92 to 1.96 cpd) which sits atop a much broader "Outer Lorentzian" (from roughly 1.75 to 2.10 cpd). See the manuscript for more details.

Results: Properties of the non-phase-locked M_2 variability

Summary of Lorentzian Parameters in the Semidiurnal Band: Parameters are obtained from nonlinear least-squares fits of a Lorentzian model for an "Inner Lorentzian" between 1.90 cpd and 1.97 cpd (columns 3-5) and for an "Outer Lorentzian" between 1.65 cpd and 2.2 cpd (columns 6-8). The $\overline{\sigma}^2$ parameter is the variance of the phase locked tide, the sum of M_2 and its annual moduilates for the Inner Lorentzian (column 3), and the sum of 16 semidiurnal constituents listed in the text for the Outer Lorentzian (column 6). The dash, "-", is used to indicate where no Lorentzian could be fit. Note that latitude ranges overlap.

		Inner Lorentzian			Outer Lorentzian		
	Area 10^6 km^2	$\overline{\sigma}^2$ cm^2	A cm^2	λ^{-1} days	$\overline{\sigma}^2$ cm^2	A cm^2	λ^{-1} days
$-60°$ to $-30°$	85	0.12	-	-	0.21	-	-
$-45°$ to $-15°$	91	0.34	-	-	0.50	0.60	26
$-30°$ to $0°$	93	0.46	0.28	209	0.66	0.86	35
$-15°$ to $15°$	94	0.39	0.46	151	0.58	1.20	35
$0°$ to $30°$	84	0.42	0.53	162	0.61	1.24	35
$15°$ to $45°$	63	0.41	-	-	0.60	-	-
$30°$ to $60°$	39	0.14	-	-	0.30	-	-
$-30°$ to $30°$	176	0.44	0.41	168	0.64	1.05	34
$-60°$ to $60°$	300	0.37	0.29	234	0.54	0.95	31

Summary & Further Questions 1

(1) The temporal autocovariance function of sea level anomaly, estimated from a combination of Jason- and CryoSat-2 mission data, provides a novel statistic for estimating the spectrum of high-frequency sea level which avoids the temporal aliasing common in analysis of mono-mission data. The relatively sparse sampling on orbit crossovers does necessitate the use of spatial averaging and introduces other forms of aliasing, though, so the usefulness of the dual-satellite autocovariance estimate is rather limited.

(2) The presence of a “tidal cusp” around the M_2 frequency is evident in the sea level anomaly spectrum, and its properties vary spatially in a manner which is consistent with previous inferences about non-phase-locked baroclinic tidal variability.

(3) The non-phase-locked variability can be characterized in terms of two different time scales, approximately 35-days and 170-days.

Summary & Further Questions 2

(4) Presumably the different timescales of variability are related to scattering by mesoscale eddies and seasonal variability in currents and stratification; although, this is a hypothesis which could be refined and tested.

(5) It would be interesting to compare, in detail, the spatially-averaged metrics for non-phase-locked tidal variability found here with those from models which resolve both baroclinic tides and mesoscales.

(6) The decorrelation timescales found here should be useful for the design of Gauss-Markov estimators for mapping or disentangling tidal and mesoscale variability from observations.

THE END

Thank you for your interest.

Abstract

It is well-known that the power spectral density of a random process may be estimated from its autocovariance function. Here I report on efforts to compute the spatially-averaged frequency spectrum and autocovariance of sea level from dual-satellite crossover data. By averaging over all crossover locations, and by using time-lagged sea level differences binned with hourly resolution, combined Jason and Cryosat-2 data yield power spectral density estimates with a Nyquist frequency of 0.5 cycles-per-hour. While the same sea surface is observed by the Jason missions and Cryosat-2, their data are contaminated by independent realizations of measurement noise, so some aspects of the autocovariance are interpreted differently than in conventional time series analysis. Because the crossover locations are not randomly distributed in space and time, there are artifacts related to the aliasing of spatial signals that appear in the frequency domain. Nonetheless, the resulting power spectral estimates clearly exhibit unaliased peaks due to high-frequency sea level above the 1/20-day Nyquist frequency associated with Jason. I will provide examples of these spectral estimates and show how they may be used to learn about non-phase-locked baroclinic tides.